PHYSICAL REVIEW E **81**, 020702(R) (2010)

Convection-roll instability in spite of a large stabilizing torque

Pramoda Kumar
Centre for Liquid Crystal Research, Professor U.R. Rao Road, P.B. No. 1329, Jalahalli, Bangalore 560 013, India

Jana Heuer
Institut für Experimentelle Physik, Otto-von-Guericke-Universität Magdeburg, Universitätsplatz 2, D-39106 Magdeburg, Germany

Tibor Tóth-Katona,* Nándor Éber, and Ágnes Buka
Research Institute for Solid State Physics and Optics, Hungarian Academy of Sciences, P.O. Box 49, H-1525 Budapest, Hungary
(Received 2 September 2009; published 25 February 2010)

Two electroconvection (EC) pattern morphologies—a cellular and a subsequent roll pattern—have been detected in the same frequency range in a nematic with positive permittivity and conductivity anisotropies. The frequency dependences of the onset voltages and critical wave numbers have been determined both for homeotropic and planar alignments. It has been proven that both pattern morphologies have a dielectric time symmetry. We also discuss possible sources for the pattern formation in the frame of both the isotropic (Felici-Benard) mechanism, as well as the standard model of EC.

DOI: 10.1103/PhysRevE.81.020702 PACS number(s): 61.30.Gd, 47.54.−r, 47.20.Lz, 64.70.M−

Nematic liquid crystals, the simplest type of intrinsically anisotropic fluids, continue to provide model systems for a great variety of interesting nonlinear dynamical phenomena, such as optical instabilities [1], flow-induced nonlinear waves [2], critical properties of nonequilibrium phase transitions [3], and in particular electrically or thermally driven convective instabilities [4,5]. Convection in nematics has contributed substantially to our general understanding of anisotropic pattern-forming phenomena; moreover, direct transitions to isotropic convection have also been observed [6], which opened up scenarios inaccessible in simple fluids.

Here, we present a transition to an electroconvecting roll system which is not predicted by the electrohydrodynamic theory of nematic liquid crystals. Electroconvection (EC) as a primary instability has originally been observed and theoretically understood in nematics with positive conductivity anisotropy ($\sigma_a>0$) and negative dielectric anisotropy ($\varepsilon_a<0$). In this configuration the pattern-forming instability sets in from the planar alignment and the destabilization is due to the charge separation mechanism introduced by Carr and Helfrich [7], which has later been extended to a three-dimensional theory, the standard model (SM) [8]. The model also allows for a direct transition to EC in nematics with reversed signs of both anisotropies, which has been found and described experimentally [6]. In this case the onset occurs from the homeotropic state. The SM (in some cases extended with the weak electrolyte model [9] or with the flexoelectricity [10]) is capable to describe almost all primary EC instabilities observed in nematics, and even numerous secondary transitions (e.g., chevron patterns, abnormal rolls, and skewed varicose).

EC patterns have also been observed for the same signs of the two relevant anisotropies. Recently, a system with $\varepsilon_a<0$ and $\sigma_a<0$—showing a direct transition to EC from the planar state—has been analyzed in more detail [11]. The scenario has been understood and reproduced quantitatively by adding flexoelectricity to the SM [10].

EC has also been reported for the other combination ($\varepsilon_a>0$ and $\sigma_a>0$) [12–15]. These measurements have mainly been constrained to the determination of thresholds versus ε_a and σ_a, as well as temperature. Depending on the driving frequency f, two distinct patterns have been detected: the fingerprint structure at low f and Maltese crosses (not considered in this Rapid Communication) at higher f [13,14]. A third type of instability, namely, the cellular pattern has also been observed, however, only at dc and below 1 Hz ac driving [16]. The isotropic (Felici-Benard) mechanism has been proposed by several authors to explain the observed instabilities [12–16]; however, a rigorous theoretical formulation of this mechanism, which is capable to provide the main pattern characteristics, is not yet available. Our aim is to give a more complete experimental description (including the wave number and the temporal evolution within one period of the driving voltage of the patterns besides the threshold measurements) in order to motivate further theoretical analysis.

We have used 4-cyano-(4′-pentyl)biphenyl (5CB) in homeotropic and planar samples of thickness $d\approx 20$ μm. A sinusoidal ac voltage of frequency f and amplitude $\sqrt{2}U$ has been applied. The samples have been thermostatted at (30 ± 0.05) °C. At this temperature 5CB has $\varepsilon_a=\varepsilon_{\parallel}-\varepsilon_{\perp}=+11.76$ [17] and we have measured $\sigma_a/\sigma_{\perp}=(\sigma_{\parallel}-\sigma_{\perp})/\sigma_{\perp}=+0.45$. EC patterns have been studied by polarizing microscope with two crossed (or nearly crossed) polarizers. Images have been recorded by a digital camera with an adjustable exposure time.

EC has been seen at homeotropic as well as at planar boundary alignment. However, the direct transition from the homogeneous state to EC requires homeotropic configuration. In the case of planar cells this requirement realizes via the Freedericksz transition [12].

On increasing the voltage applied to the *homeotropically* aligned cell, flow (i.e., migration of particles) can be observed at relatively low voltages; above that a direct transi-

*Corresponding author; katona@szfki.hu

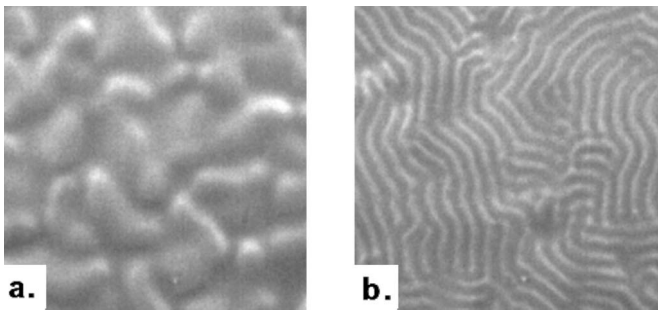

FIG. 1. Snapshots of the convective patterns at $f=12$ Hz slightly above the threshold voltage in a homeotropic sample of $d=20.2$ μm. (a) Cellular pattern, $U=10.6$ V; (b) roll pattern, $U=13.6$ V. The images are 300×300 μm^2 in size.

tion to EC occurs. The first instability is a two-dimensional (2D) cellular structure with a large wavelength. It consists of slightly deformed round shaped cells demonstrated in Fig. 1(a). This pattern becomes dynamic and evolves with increasing voltage toward a quasihomogeneous state. The second distinct morphology, a roll structure (fingerprint), emerges at higher threshold with a lower wavelength [see Fig. 1(b)]. Rolls are disordered because there is no preferred direction in the plane of the structure.

The properties of the rolls contrasted by the standard EC structures (predicted by SM) are as follows: (i) the pattern can only be visualized between crossed or nearly crossed polars, thus no shadowgraph image is seen; (ii) the patterns form in a relatively low frequency range, typically below 100 Hz; and (iii) an unusually broad stability region of the rolls above threshold has been detected [up to $\epsilon=(U/U_c)^2-1\approx2$].

The frequency dependence of the threshold voltage U_c and that of the dimensionless critical wave number $q_c=2d/\lambda_c$ (λ_c is the wavelength) of both (the cellular as well as the roll) patterns are shown in Figs. 2(a) and 2(b). $U_c(f)$ of both structures follows a similar behavior, namely, a square-root-type frequency dependence, typical for the standard dielectric EC mode. q_c of the *cellular structure* is almost independent of the frequency and corresponds to a wavelength of about $\lambda_c\approx(3-4)d$. The fairly large error bars reflect the irregularity of the pattern as seen in Fig. 1(a). $q_c(f)$ of the *rolls* roughly follows the $U_c(f)$ curve and gives a wavelength in the range of $(0.6-1)d$.

In the *planarly* aligned samples, due to $\varepsilon_a>0$, the first instability is the homogeneous splay Freedericksz transition at $U_F\approx0.8$ V to a quasihomeotropic state where the director in the bulk of the sample is basically aligned parallel to the electric field, and only thin layers at the boundaries contain a splay-bend deformation zone. Further increasing the voltage the scenario is qualitatively similar to that in the homeotropic case; a cellular structure emerges which is followed by an ordered roll pattern as shown in Figs. 3(a) and 3(b). Figures 4(a) and 4(b) present $U_c(f)$ and $q_c(f)$, respectively. The general qualitative properties of the patterns at the onset given previously for the homeotropic alignment apply here as well.

Comparing the characteristics of the patterns observed in homeotropic and planar cells one can conclude that the cellular pattern does not seem to be influenced by the boundary

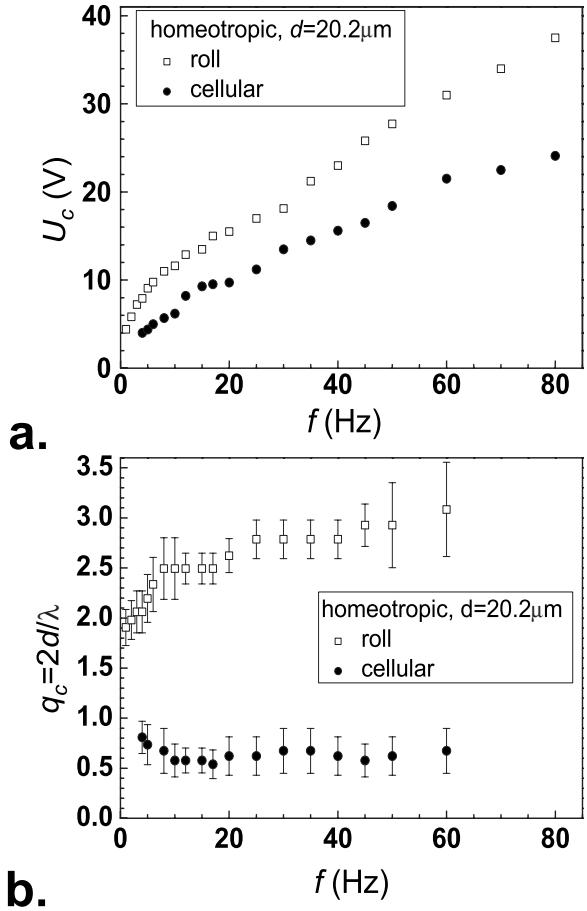

FIG. 2. Frequency dependence (a) of the threshold voltage U_c and (b) of the critical wave number q_c for both the cellular and the roll patterns, measured in a homeotropic sample of $d=20.2$ μm at $T=30$ °C.

condition. Namely, its 2D image, threshold, and wave number are very similar for the two alignments. This is not surprising since $U_c\gg U_F$.

In contrast to the cellular pattern, the rolls are very sensitive to the boundary conditions, even though they have a higher threshold. The critical wave numbers of the rolls do not differ significantly for the two alignments, but the rolls

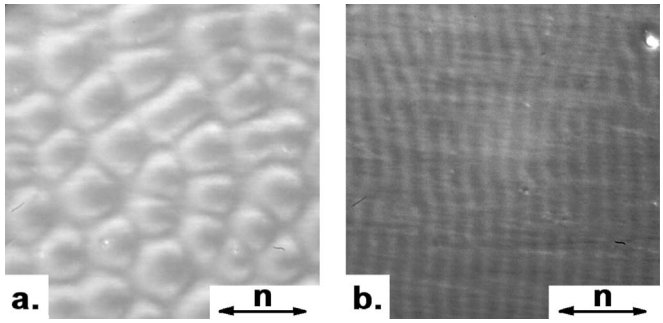

FIG. 3. Snapshots of the convective patterns at $f=4$ Hz slightly above the threshold voltage in a planar sample of $d=19.5$ μm. (a) Cellular pattern, $U=7.2$ V; (b) roll pattern, $U=14.4$ V. Double arrows indicate the initial director. The images are 300×300 μm^2 in size.

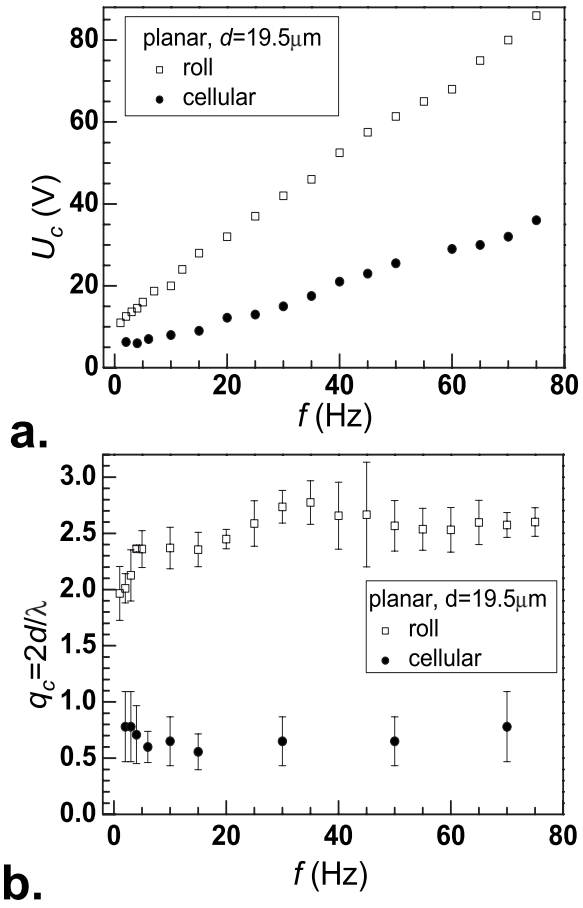

FIG. 4. Frequency dependence (a) of the threshold voltage U_c and (b) of the critical wave number q_c for both the cellular and the roll patterns, measured in a planar sample of $d=19.5$ μm at $T=30$ °C.

become oriented normal or slightly oblique to the rubbing direction for the planar case. We have to draw the attention to the unusually large (about a factor of 2) difference between the roll thresholds in the homeotropic and in the planar cases. The large influence of the boundaries on the rolls is a counterintuitive fact, taking into account that the rolls set in from a similar state in both alignments, which originates from the cellular structure. One possible explanation for this unexpected feature could be that the cellular structure forms in the bulk, while the rolls form at the boundaries. Experiments have also been performed in which the xy-focal plane has been varied in the z direction in ≈ 3 μm steps. The midplane of the sample has been identified by observing several spacers in the cell [see the white spot in the upper right corner of Fig. 3(b)]. These "depth" measurements have revealed distinct differences between the cellular and the roll patterns. A relatively sharp image of the cellular pattern has appeared around the midplane of the cell in a z band slightly larger than d. In contrast, relatively sharp images of the roll pattern have been found in two z bands (below and above the sample) separated by an ≈ 20 μm gap in which the pattern is unfocused.

An important question concerning the nature of the pattern is its time symmetry, i.e., whether the director does or

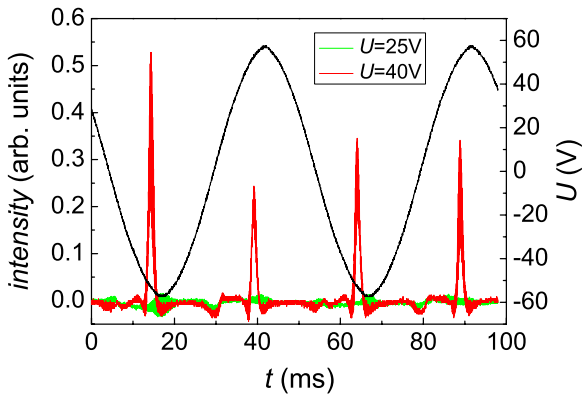

FIG. 5. (Color online) Temporal evolution of the first-order diffraction fringe intensity for the roll pattern in a 19.5-μm-thick planar 5CB at $f=20$ Hz, $T=30$ °C. Below onset ($U=25$ V) the intensity is nearly constant; above onset ($U=40$ V) bursts are present in each half-period. The sine curve represents the driving voltage.

does not oscillate with the driving frequency. In the standard EC these two regimes are called "dielectric" and "conductive," respectively. In order to decide, we have varied the exposure time of our camera. The pattern could be safely detected by snapshots only if the exposure lasted at least about the half-period of the exciting ac voltage; for shorter exposure time the pattern faded away. This indicates that the pattern does not exist stationarily; rather it emerges and decays again within each half-period, i.e., the pattern is of dielectric type. This statement holds for both initial alignments. A confirmation of this conclusion could be obtained by monitoring the temporal behavior of the intensity of the first-order diffraction fringe in planar cells illuminated by a laser. Figure 5 depicts the time dependence of the intensity for the roll pattern for two periods of the driving voltage. It is seen that the diffracted light intensity appears as a sequence of bursts occurring twice within one period; i.e., in most of time the pattern does not exist. A similar behavior has been observed recently in the standard EC, but only at very low frequencies ($f<1$ Hz) [18] where the period of the driving signal is much larger than the director relaxation time τ_d. The surprising feature in our case is that bursts are observable up to quite high frequencies (>50 Hz$\gg\tau_d^{-1}$). The other surprising feature here is that the phase shift between the bursts and the driving voltage appears to be independent of f, in contrast to the case in the standard dielectric EC [18].

Another important question is the driving mechanism of these instabilities. The standard EC model predicts roll formation if the signs of ε_a and σ_a are different. Moreover, EC roll patterns found for $\varepsilon_a<0$, $\sigma_a<0$ have also been described by the extended SM, i.e., by adding flexoelectricity. In that case, the standard Ohmic charge separation mechanism is blocked by the negative σ_a, which can be compensated (and overtaken) by the flexoelectric charge.

As we have tested, the inclusion of flexoelectricity does not bring similar (or any) effect here, because flexoelectricity does not couple in leading order to the nematoelectrohydrodynamic equations for homeotropic boundary conditions. However, the destabilizing force must be very robust, because it overtakes the strong stabilizing dielectric torque due to the large positive ε_a.

We have also considered the "test function approximation" of the SM and analyzed the one-mode analytical threshold formula labeled as case C in Eqs. (6.29)–(6.33) of Ref. [4] (see [19]). On one hand the formula predicts a direct convective destabilization from the homeotropic alignment for positive ε_a calculated for 4-methoxy-benzylidene-4′-*n*-butyl-aniline (MBBA) material parameters, but the threshold diverges at very low positive ε_a. Using 5CB parameters [5,12] this solution branch did not extend to higher ε_a values either. On the other hand, the term $\tilde{\sigma}_a^{(eff)}$ becomes negative for 5CB (see [19]); thus, it may off balance the effective dielectric contribution in Eq. (6.29.) of Ref. [4], leading to a new solution branch, never considered before. Indeed, we have obtained the EC onset at $U_c \approx 12$ V and $q_c \approx 18$ for $f=50$ Hz with a parameter set close to that of 5CB. We want to emphasize, however, that besides the high value of q_c (corresponding to a wavelength of ≈ 2 μm), one has to handle this result with an extreme care. The analytical threshold expression of the one-mode approximation might give solutions that are unstable if one includes higher modes. Therefore, a complex detailed numerical analysis is necessary in the future to clarify this otherwise promising result.

We are convinced that the isotropic Felici-Benard model in its presently available state cannot give an acceptable solution here. We have estimated the threshold voltage for the more realistic bipolar injection (Eq. (4) of Ref. [13]) and obtained a very high $U_c \approx 200$ V, while for the unipolar injection (Eq. (3) of Ref. [13]) a very low—thickness-independent—threshold occurs at $U_c \approx 1$ V, which is comparable to the Freedericksz threshold. Obviously, none of these values agree with the experiments. Moreover, the model does not go beyond a one-dimensional description; thus, no wave-vector prediction is available—except the Debye screening length of ~ 10 nm, which is too small compared to the measured wavelengths.

Some future experiments should reveal the source of the large difference in U_c for the homeotropic and planar boundary conditions, and explore in detail the differences between the cellular and the roll patterns. Confocal polarizing microscopy [20] and "storing" the patterns via photopolymerization followed by investigations by atomic force microscopy [21] might be useful tools to bring us closer to understanding the two presumably different driving mechanisms that result in disparate patterns.

We thank R. Stannarius, W. Pesch, and A. P. Krekhov for fruitful discussions, and M. Bordo, B. Kautz, and D. Statman for their contribution to Fig. 5. Financial support by the Hungarian Research Fund Contracts No. OTKA-K61075 and No. K81250 is gratefully acknowledged. P.K. acknowledges the financial support from INSA and HAS; he is also thankful to K. A. Suresh, K. S. Krishnamurthy, and S. Krishna Prasad.

[1] G. Demeter and D. O. Krimer, Phys. Rep. **448**, 133 (2007).
[2] J. T. Gleeson, P. Palffy-Muhoray, and W. van Saarloos, Phys. Rev. A **44**, 2588 (1991); T. Börzsönyi, Á. Buka, A. P. Krekhov, O. A. Scaldin, and L. Kramer, Phys. Rev. Lett. **84**, 1934 (2000).
[3] P. K. Mukherjee, J. Phys.: Condens. Matter **10**, 9191 (1998); S. Singh, Phys. Rep. **324**, 107 (2000).
[4] L. Kramer and W. Pesch, in *Pattern Formation in Liquid Crystals*, edited by Á. Buka and L. Kramer (Springer-Verlag, New York, 1996), p. 221.
[5] G. Ahlers, in *Pattern Formation in Liquid Crystals*, edited by Á. Buka and L. Kramer (Springer-Verlag, New York, 1996), p. 165.
[6] A. Buka *et al.*, Phys. Rev. E **66**, 051713 (2002); A. Buka, B. Dressel, L. Kramer, and W. Pesch, Phys. Rev. Lett. **93**, 044502 (2004); Chaos **14**, 793 (2004).
[7] E. F. Carr, Mol. Cryst. Liq. Cryst. **7**, 253 (1969); W. Helfrich, J. Chem. Phys. **51**, 4092 (1969).
[8] E. Bodenschatz *et al.*, J. Phys. (France) **49**, 1875 (1988).
[9] M. Treiber and L. Kramer, Mol. Cryst. Liq. Cryst. Sci. Technol., Sect. A **261**, 311 (1995).
[10] A. Krekhov, W. Pesch, N. Eber, T. Toth-Katona, and A. Buka, Phys. Rev. E **77**, 021705 (2008).
[11] E. Kochowska, S. Nemeth, G. Pelzl, and A. Buka, Phys. Rev. E **70**, 011711 (2004); T. Tóth-Katona, A. Cauquil-Vergnes, N. Éber, and Á. Buka, *ibid.* **75**, 066210 (2007).
[12] L. M. Blinov and V. G. Chigrinov, *Electrooptic Effects in Liquid Crystal Materials* (Springer, Berlin, 1996).
[13] M. I. Barnik *et al.*, Sov. Phys. JETP **45**, 396 (1977); A. N. Trufanov *et al.*, Zh. Eksp. Teor. Fiz. **80**, 704 (1981).
[14] D. K. Rout and R. N. P. Choudhary, Liq. Cryst. **4**, 393 (1989).
[15] E. I. Rjumtsev and S. G. Polushin, Liq. Cryst. **13**, 623 (1993).
[16] M. Nakagawa and T. Akahane, J. Phys. Soc. Jpn. **52**, 3773 (1983); **52**, 3782 (1983).
[17] H. J. Coles and M. S. Sefton, Mol. Cryst. Liq. Cryst., Lett. Sect. **4**, 123 (1987).
[18] M. May, W. Schöpf, I. Rehberg, A. Krekhov, and A. Buka, Phys. Rev. E **78**, 046215 (2008).
[19] Equation (6.31) of Ref. [4] is misprinted. The proper equation reads as $\tilde{\sigma}_a^{(eff)} = (\sigma_a \epsilon_\perp / \epsilon_\parallel)[1 - (\epsilon_a \sigma_\perp / \epsilon_\perp \sigma_a)]/[(1+\omega'^2)\tilde{S}]$.
[20] N. Gheorghiu, I. I. Smalyukh, O. D. Lavrentovich, and J. T. Gleeson, Phys. Rev. E **74**, 041702 (2006).
[21] A. Hoischen *et al.*, Appl. Phys. Lett. **93**, 131903 (2008); J. Appl. Phys. **105**, 013540 (2009).